ISSN 0915-633X

NATIONAL INSTITUTE FOR FUSION SCIENCE

Electron Cyclotron Current Drive at $\omega \approx \omega_c$ with X-mode Launched from the Low Field Side

F. Leuterer and S. Kubo

(Received - Jan. 14, 2000)

NIFS-624 Feb. 2000

RESEARCH REPORT
NIFS Series

NAGOYA, JAPAN

Electron Cyclotron Current Drive at $\omega \approx \omega_c$ with X-mode Launched from the Low Field Side

F. Leuterer *, S. Kubo **

* *Max Planck Institut für Plasmaphysik, D-85740 Garching, Germany*

** *National Institute for Fusion Science, Toki-shi, Gifu-ken 509-5292, Japan*

Abstract

The electron cyclotron resonance layer in a tokamak, $\omega = \omega_c(r)$, is not accessible by the extraordinary wave from the low field side, because it is shielded by a cutoff layer. However, a X-mode launched with a nonzero toroidal angle propagates at the cutoff parallel to the magnetic field and has a circular polarization. Therefore it can already at the cutoff layer interact efficiently with electrons via the Doppler shifted resonance. The driven current can be substantially higher than that driven by the second harmonic X-mode. The applicability of this current drive scheme is limited to rather low values of ω_p^2/ω_c^2, but may be of interest for high magnetic field devices.

Keywords: electron cyclotron current drive, extraordinary wave

1. Introduction

Electron cyclotron current drive scenarios for tokamaks use the fundamental ordinary mode (O1-mode) or the second harmonic extraordinary mode (X2-mode) launched from the low field side. In earlier experiments also the X1-mode launched from the high field side was used [1, 2]. These schemes differ in the location in velocity space where power is absorbed, and in the power absorbed per single electron. O1-mode and X2-mode launched from the low field side are chosen mainly because of their large optical thickness, which increases linearly with temperature leading to full single pass absorption of the incident wave, and because low field side launching is technically simpler. In both cases the absorbed power per single electron is due to its finite gyroradius.

A scenario which has apparently been neglected in the studies of ECCD is current drive near the fundamental cyclotron frequency with an X1-mode launched from the low field side. The reason is that for extraordinary waves the electron cyclotron resonance region in a tokamak, $\omega = \omega_c(r)$, is only accessible when they are launched from the high field side, where $\omega < \omega_c(r)$. From the low field side, where $\omega > \omega_c(r)$, the resonance is shielded by a cutoff region as shown in the CMA diagram in Fig. 1. However, when the extraordinary wave propagates obliquely to the magnetic field we do not need to access the resonance region for an efficient damping and current drive [3, 4, 5]. In this paper we discuss the prospects and limits of such an ECCD scheme.

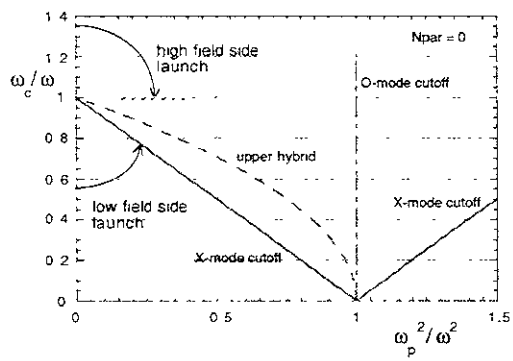

Fig. 1: High field and low field side launch in the CMA diagram.

2. X-mode propagation from the low field side

According to the resonance condition for electron – wave interaction there can be a considerable shift of the absorption region towards the lower magnetic field side because of the relativistic effect combined with the Doppler shift. This resonance condition is

$$\omega = n \cdot \gamma \, \omega_c + k_{\parallel} \cdot v_{\parallel} \qquad (1)$$

where $\gamma = \sqrt{1 - v^2/c^2}$ is the relativistic factor, $\omega_c = eB/m$ is the nonrelativistic cyclotron frequency,

and n is the harmonic number. In this paper we consider only the case $n = 1$.

Introducing $V = v/c$ and $N_{\parallel} = k_{\parallel} c/\omega$ we can rewrite Eq. (1) in the form

$$V_{\perp}^2+\left(1+N_{\parallel}^2\cdot(\omega^2/\omega_c^2)\right)\cdot\left(V_{\parallel}-\frac{N_{\parallel}\cdot(\omega^2/\omega_c^2)}{1+N_{\parallel}^2\cdot(\omega^2/\omega_c^2)}\right)^2=1-\frac{(\omega^2/\omega_c^2)}{1+N_{\parallel}^2\cdot(\omega^2/\omega_c^2)} \qquad (2)$$

which is the equation of an ellipse in the velocity space coordinates $V_{\perp}$ and $V_{\parallel}$, describing the positions in velocity space where an electron can absorb energy from a wave with given ω/ω_c and $N_{\parallel}$.

This is shown in Fig. 2, where we assume a fixed value of $N_{\parallel} \neq 0$. For $N_{\parallel} = 0$ the ellipses become circles centered around the origin. For $\omega/\omega_c = 1$ and $N_{\parallel} \neq 0$ the resonant ellipse passes through the origin. Outside of this one are those for $\omega/\omega_c < 1$, while those for $\omega/\omega_c > 1$ are inside of it.

In a tokamak the toroidal magnetic field is proportional to $1/R$, and therefore the space coordinate R can also be seen as a ω/ω_c – coordinate. Waves coming from the high field side are first interacting with electrons along the resonant ellipses for $\omega/\omega_c < 1$, while waves coming from the low field side are first interacting with electrons along the $\omega/\omega_c > 1$ ellipses. The boundaries of the cutoff region in real space, given by the upper hybrid resonance condition

$$\omega^2/\omega_c^2 = \omega_p^2/\omega_c^2 + 1 \quad , \qquad (3)$$

and the X-mode cutoff condition

$$\left(\omega/\omega_c\right)_{c.o} = \frac{1}{2}\left(1+\sqrt{1+4\left(\omega_p^2/\omega_c^2\right)/\left(1-N_{\parallel}^2\right)}\right) \qquad (4)$$

can also be transformed into a corresponding cutoff region in velocity space. This is shown in Fig. 3, where we also see that the thermal electrons around the origin are shielded, and only the electrons in the region bounded by the cutoff can be heated by waves coming from the low field side.

From Figs. 2 and 3 we see that there is a maximum value for ω/ω_c for which resonant electrons exist and absorption is possible. From Eq. (1), we obtain for this value

$$\left(\omega/\omega_c\right)_{max} = \frac{1}{\sqrt{1-N_{\parallel}^2}} \quad , \qquad (5)$$

and the corresponding electron energy is

$$\left(V_{\parallel}^2\right)_{max} = N_{\parallel}^2 \quad . \qquad (6)$$

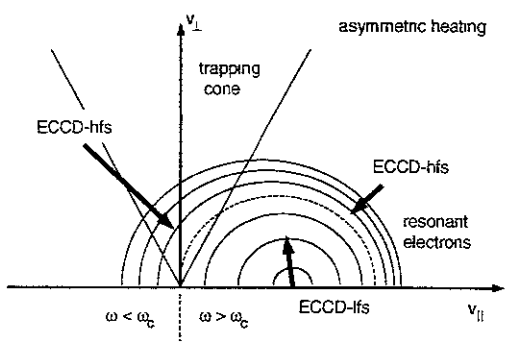

Fig. 2: ECRH from high field side vs. low field side

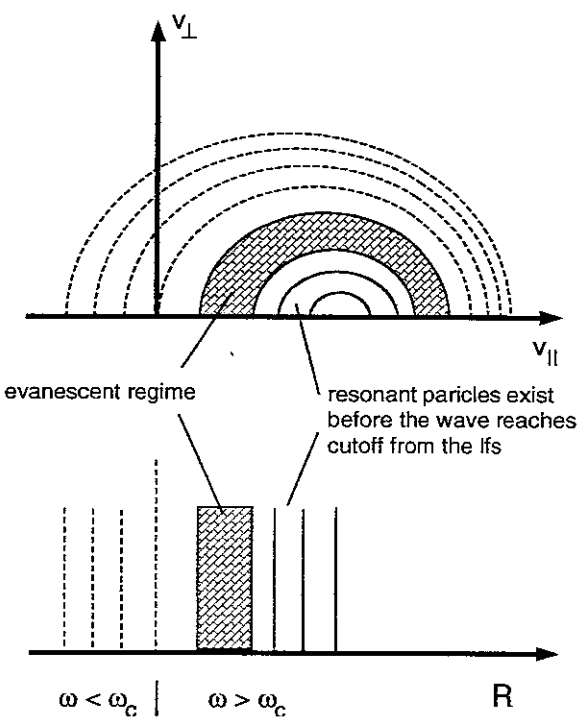

Fig. 3: The cutoff region in real space leads to a cutoff region in velocity space

There is also a minimum electron energy for which absorption is possible with $\omega/\omega_c > 1$. This is the lower $V_{\parallel}$ point of the X-mode cutoff boundary $\omega/\omega_c = (\omega/\omega_c)_{co}$ in Fig. 3, which is given by

$$\left(V_{\parallel}^2\right)_{min} = \left(\frac{AN_{\parallel} - \sqrt{AN_{\parallel}^2 - A + 1}}{AN_{\parallel}^2 + 1}\right)^2 \qquad (7)$$

with $A = \left(\omega^2/\omega_c^2\right)_{co}$.

For absorption to be possible, we must have

$$\left(\omega/\omega_c\right)_{max} > \left(\omega/\omega_c\right)_{co} , \qquad (8)$$

This leads to a maximum possible density at which absorption is possible for a given local value of $N_{\parallel}$

$$\left(\omega_p^2/\omega_c^2\right)_{limit} = 1 - \sqrt{1 - N_{\parallel}^2} \quad . \qquad (9)$$

For $N_{\parallel} = 0.6$ this leads to $\omega_p^2/\omega_c^2 = 0.2$, which corresponds to a pretty low, although local, density, for example $1.7 \cdot 10^{19}$ m^{-3} in a 3 T magnetic field. This density limit increases quadratically with the magnetic field, and in a high magnetic field device it can reach values typical in present day tokamaks.

There is another argument which makes this scheme attractive. At the cutoff the wave propagates parallel to the magnetic field and it is circularly polarized, the electric field vector rotating in the same direction as the electrons. The absorption is not a finite gyro-radius effect like in the cases of fundamental O-mode or second harmonic X-mode. Only electrons with supra-thermal parallel velocities, but already at relatively low $v_{\perp}$, show considerable absorption. Thermal electrons are shielded by the cutoff. Provided that there are a sufficient number of resonant electrons at the cutoff layer there may be good overall absorption. An experiment of this kind was performed in the WT-3 tokamak, where the necessary fast electrons were provided by simultaneous application of lower hybrid current drive [4, 5].

3. X1-mode low field side launch example for ASDEX Upgrade

We have done a calculation for off axis current drive with X1-mode low field side launching in a low density and high electron temperature plasma with high magnetic field using ASDEX Upgrade geometry (R_0 = 1.65 m, a = 0.5 m, elongation ≈ 1.5), and compared it to current drive with X2-mode low field side launching [3]. The parameters are f = 140 GHz, $n_e(0) = 2 \cdot 10^{19}$ m^{-3} with

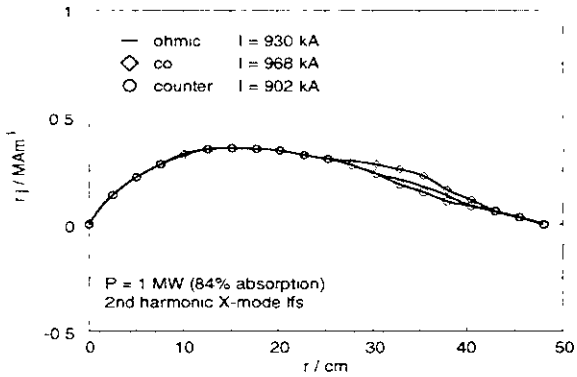

Fig.4: Current distribution for off-axis ECCD in the X2-mode, B = 1.82 T

a flat profile, $n_e(\rho)/n_e(0) = (1-\rho^2)^{0.5}$, and $T_e(0)$ = 5 keV with a peaked profile, $T_e(\rho)/T_e(0) = (1-|\rho|)^{0.9}$, $\rho = r/a$. The launched power is 1 MW. The launch angle is 25° with respect to the radial direction in the mid-plane of the torus, which corresponds to $N_{//}(a) = 0.42$ at the plasma edge. The magnetic field on the magnetic axis is 3.4 T in the first case, and 1.82 T in the second harmonic case. This places the center of the power deposition on the high field side of the magnetic axis at ρ = 0.7. The local density and temperature are $1.5 \cdot 10^{19}$ m^{-3} and 1.5 keV. The calculations have been performed with the BANDIT-3D code [6]. In Fig. 4 we plot the driven current density j in the second harmonic case, multiplied by the radius r. The ECCD current is 38 kA in the co-direction, and the single pass power absorption is 84%. The driven current is rather moderate, which is explained by the finite gyro-radius absorption mechanism and a strong influence of trapped electrons.

This is quite different for the fundamental frequency case. Figure 5 shows the result of the same calculation, except that the magnetic field was

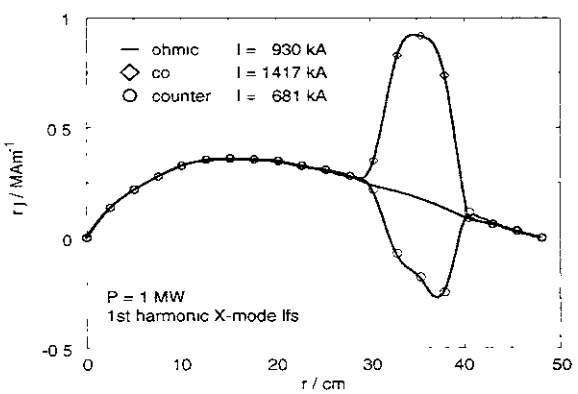

Fig.5: Current distribution for off-axis ECCD in the X1-mode, B = 3.4 T

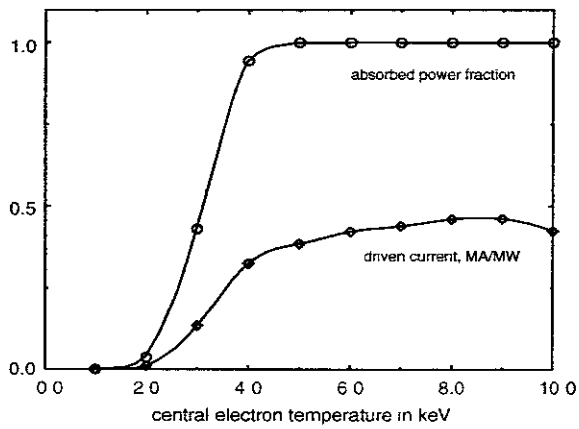

Fig. 6: Electron temperature threshold for the onset of X1-mode current drive

raised to 3.4 T. Here the ECCD driven current is 487 kA in co-direction and the single pass absorption is 100%. The driven current is an order of magnitude larger than in the previous case of second harmonic ECCD.

This example shows that already at a temperature of 1.5 keV at the absorption layer there is a sufficient supra-thermal electron population in velocity space to allow for complete absorption of the incident wave. Figure 6 shows the dependence of absorbed power and driven current on the central electron temperature, keeping all other parameters fixed as in the example of Fig. 5. Note that, for the chosen profile, the temperature at the absorption layer is only about one third of the central temperature. There is a temperature threshold at $T_e(0) \approx 2$ keV. But already at a central temperature of 4.5 keV the power is fully absorbed, and with even higher temperature the current increases only slightly. Finally the driven current decreases again due to the beginning of second harmonic X-mode absorption at the low field side. This problem can be avoided if the wave is launched from a top position instead of a mid-plane position.

4. Discussion

The feasibility of this scheme can be studied by plotting the quantities $\omega/\omega_c \sim 1/R$, $(\omega/\omega_c)_{c.o.}$, and $(\omega/\omega_c)_{max}$ as a function of normalized minor radius ρ. For the density profile we take $n_e(\rho) = n_e(0)\cdot[1-(\rho)^4]$ and for the aspect ratio we take 3.3. Furthermore we assume launching from the low field side mid-plane, and we neglect the poloidal magnetic field, so that $N_{\parallel} = N_{tor} \sim 1/R$. In Fig. 7 this is done for the case of Fig. 5, for which the normalized central density and central frequency are $\omega_p^2/\omega_c^2(0) = 0.175$ and $\omega/\omega_c(0) = 0.145$. Coming from the low field side ω/ω_c decreases and first

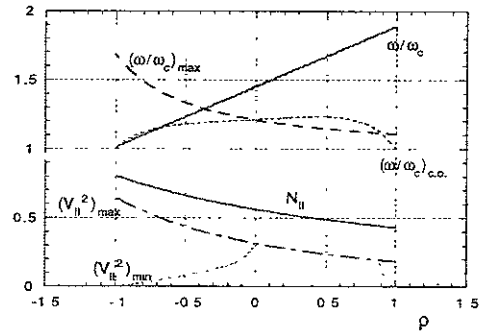

Fig. 7: Cold plasma model, ω/ω_c (0) = 1.45, $N_{\parallel}(1) = 0.43$, $\omega_p^2/\omega_c^2(0) = 0.175$

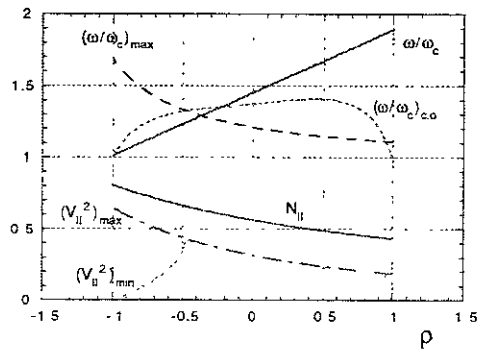

Fig. 8: Same as Fig. 7, but $\omega_p^2/\omega_c^2(0) = 0.35$

encounters the intersection with the line $(\omega/\omega_c)_{max}$ and only later reaches the cutoff line $(\omega/\omega_c)_{c.o.}$. This means that absorption is possible before the wave reaches the cutoff and is reflected. Thus an absorption window $(\omega/\omega_c)_{max} > \omega/\omega_c > (\omega/\omega_c)_{c.o.}$ exists in real space and in velocity space. The width and the location of this window depend on density, magnetic field and toroidal launch angle, i.e. $N_{//}$, We also show in this figure the energies $(V_{\parallel}^2)_{max}$ and $(V_{\parallel}^2)_{min}$ from Eqs. (6) and (7). Figure 8 shows the same calculation as in Fig. 7, but for a higher central density of $\omega_p^2/\omega_c^2(0) = 0.35$. In this case the line for ω/ω_c first intersects the cutoff line $(\omega/\omega_c)_{c.o.}$, and only later the line for $(\omega/\omega_c)_{max}$, and therefore no absorption window exists.

In Fig. 9 we plot a summary of calculations with the parameters of Fig. 7, but with different peak densities. Fig. 9a shows the locations ρ_{max} of the $(\omega/\omega_c) - (\omega/\omega_c)_{max}$ intersection and the locations $\rho_{c.o.}$ of the intersection $(\omega/\omega_c) - (\omega/\omega_c)_{c.o.}$, representing the spatial boundaries of possible absorption. In Fig. 9b we see the corresponding values of the energies $(V_{\parallel}^2)_{max}$ and $(V_{\parallel}^2)_{min}$. Figure 5 was calculated with a real beam of finite width corresponding to a $N_{\parallel} \approx 0.43 \pm 0.03$, and in Fig. 9 we also show with the dashed lines how the absorption boundaries and

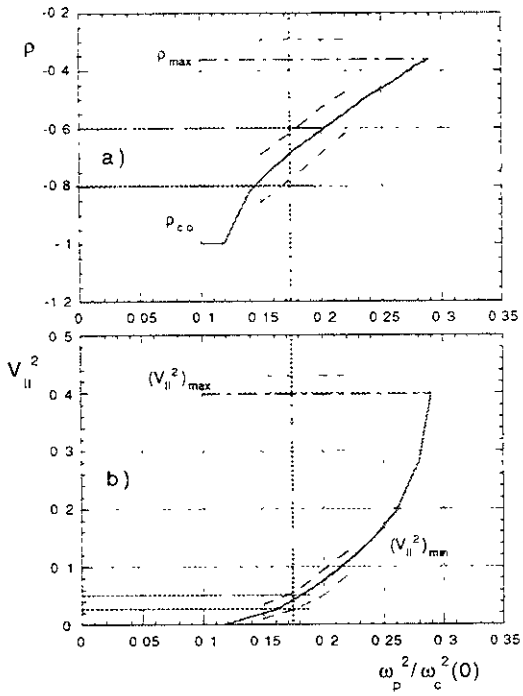

Fig. 9: a) locations of ρ_{max} and ρ_{co}, and b) associated maximum and minimum energies as function of the central density. ω/ω_c (0) = 1.45, $N_{||}(1) = 0.43 \pm 0.03$

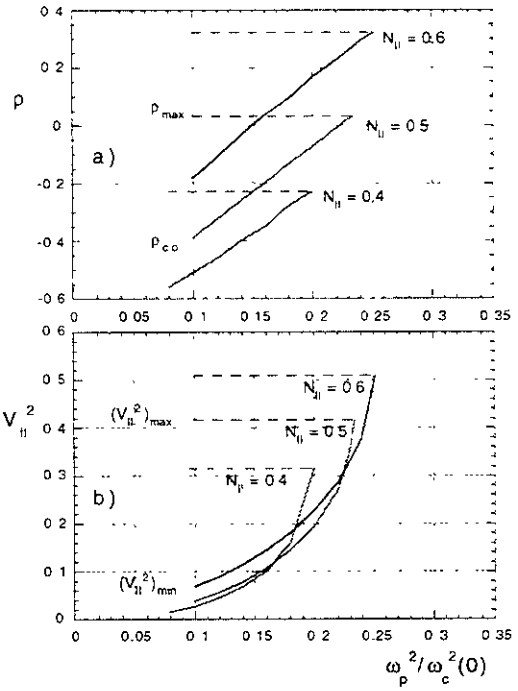

Fig. 11: Same as Fig. 9, but ω/ω_c (0) = 1.30, and various $N_{||}(1)$.

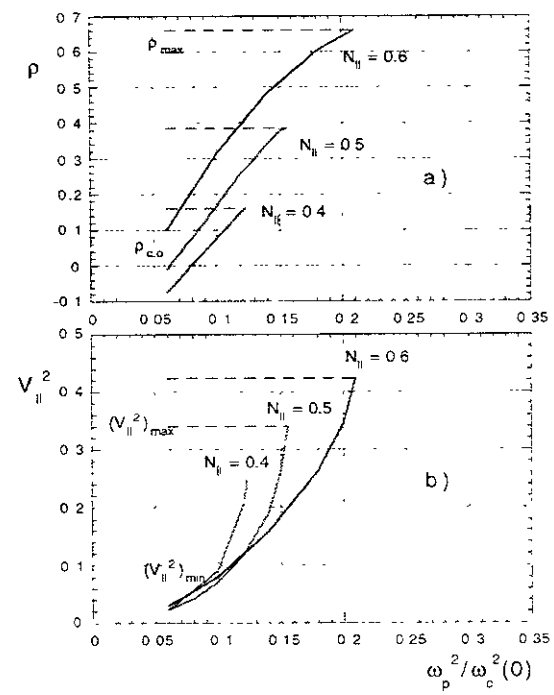

Fig. 10: Same as Fig. 9, but ω/ω_c (0) = 1.10, and various $N_{||}(1)$.

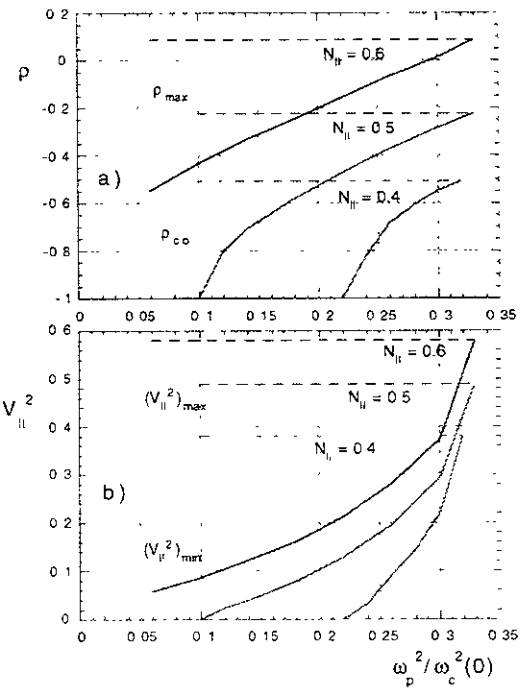

Fig. 12: Same as Fig. 9, but ω/ω_c (0) = 1.50, and various $N_{||}(1)$.

energies shift within this range of $N_{||}$. In Fig. 9 the peak density of $2 \cdot 10^{19}$ m^{-3} with which Fig. 5 was calculated, corresponds to $\omega_p^2/\omega_c^2(0) = 0.175$, The cutoff boundaries within the $N_{||}$ - spectrum coincide for this density quite well with the spatial boundaries of the driven current obtained from the Fokker-Planck calculation shown in Fig. 5 and indicated by the dotted lines in Fig. 9a, and from Fig. 9b. We then find that the minimum electron energies involved in the absorption are in the range $V_{||}^2 \approx 0.025$ to 0.05, i.e. in the tail of the local thermal distribution function. The dependence on the magnetic field and $N_{||}$ is shown in Figs. 10, 11 and 12. For a higher magnetic field and higher $N_{||}$ the interaction region shifts from high field side off-axis towards the center. For too low magnetic field there is the risk of second harmonic absorption at the low field side edge of the plasma.

5. An ITER like example

The calculations of Figs. 4, 5 and 6 have been done for a fairly low density plasma where an absorption window exists. However, since this scenario scales with ω_p^2/ω_c^2, the density limit for the absorption window to open increases quadratically with the toroidal magnetic field. We therefore did a similar calculation with the same magnetic field configuration, but with the increased major radius to R_0 = 8.5 m, the minor radius to a = 2.4 m, the magnetic field to 6 T, the central density to $9 \cdot 10^{19}$ m^{-3} and the central temperature to 15 keV. For the profiles we used $n_e(\rho)=(1-\rho^2)^{0.5}$, and $T_e(\rho)=(1-\rho^2)^{1.3}$. With a toroidal launch angle of 25° the absorption was located at $\rho \approx 0.5$, and the local density and temperature were $7.9 \cdot 10^{19}$ m^{-3} and 9.2 keV. With the wave launched in the O1-mode at 233 GHz the driven current was 20 kA/MW, while with a wave launched in the X1-mode at 240 GHz the driven current was 30 kA/MW, i.e. 50 % higher. A possible second harmonic absorption at the edge was neglected in this calculation. The resulting current profiles are shown in Fig. 13. Obviously the higher temperature, compared to the example of Fig. 5, led to a stronger finite gyro-radius absorption for the O1-mode case and the difference in the driven currents is no longer as pronounced. Nevertheless, this example shows that, although the range in density where this scheme can be applied is rather restricted, using fundamental X1-mode for off axis ECCD in ITER might result in a somewhat higher current drive efficiency than for O1-mode.

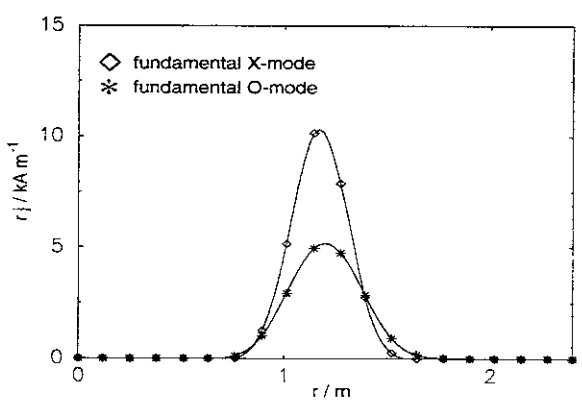

Fig. 13: Comparison between X1-mode and O1- mode current drive for ITER like parameters

6. Application to the Large Helical Device

A top view of the LHD constant magnetic field contours, flux surface contours and the available ECRH antennas in the horizontal port is

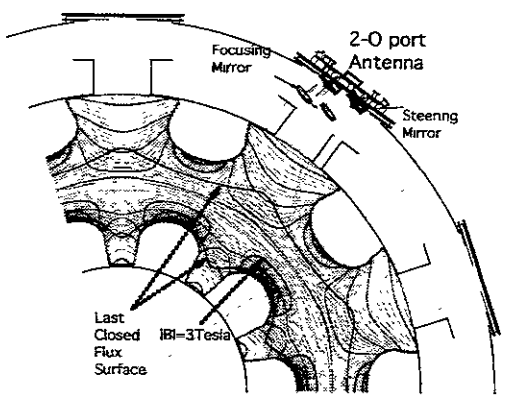

Fig. 14: Horizontal cross-section of LHD available launching mirrors. The ray is shown with the toroidal deflection of – 0.8 m.

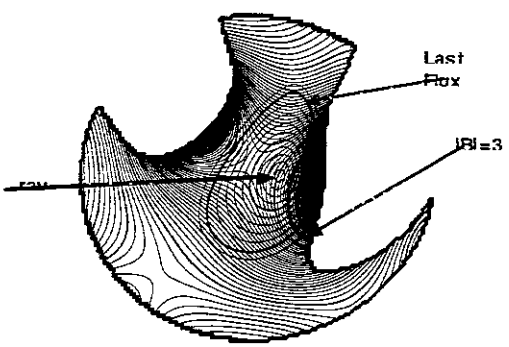

Fig. 15: Vertical cross-section of LHD along a ray with toroidal deflection of – 0.8 m.

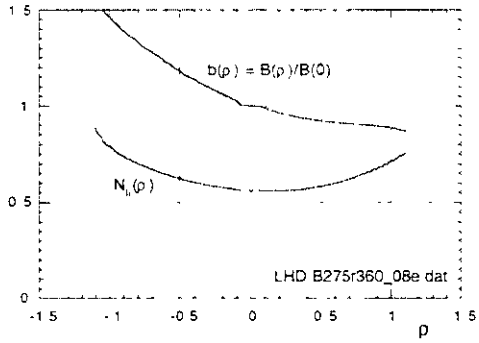

Fig. 16: Variation of magnetic field and $N_{||}$ in LHD along a ray launched from a horizontal port with toroidal deflection of – 0.8 m.

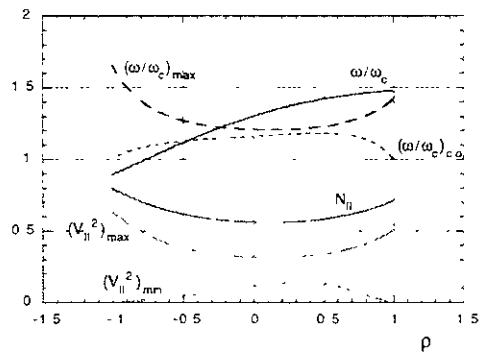

Fig. 17: Cold plasma model applied to LHD, ω/ω_c (0) = 1.30, $\omega_p^2/\omega_c^2(0) = 0.125$, toroidal ray deflection – 0.8 m.

shown in Fig. 14. The thick lines are the contours for |B| = 3 T and the outermost closed flux contour (ρ = 1) respectively. The presently installed gyrotrons of the ECRH system operate at frequencies of 82.6 GHz, 84 GHz, and 168 GHz. The lower frequencies can be used for fundamental X-mode current drive. There are also antennas installed in the vertical ports.

From the previous discussions in tokamak geometry we know that we need a high $N_{||}$ in the absorption region in order to place the interaction not too far into the tail of the distribution function. The vertical port antennas do not allow a toroidal angle scan as wide as the horizontal port antennas do. Furthermore we gain from the geometrical $1/R$ dependence of $N_{||}$ when using the horizontal port antennas. The best conditions in this respect are given for the toroidal launching positions – 0.7 m to –0.9 m. We take here as a representative case the position – 0.8 m. The vertical cross-section of the plasma along this direction is shown in Fig. 15, and Fig. 16 shows the variation of |B| and of $N_{||}$ along a ray from the antenna through the plasma center,

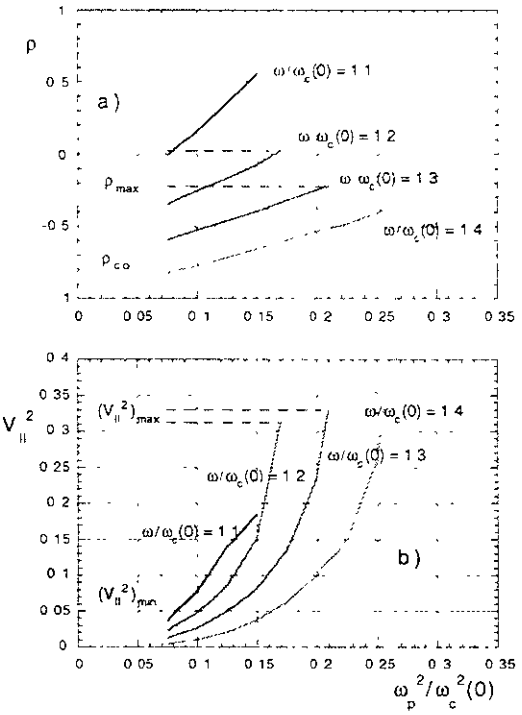

Fig.18: a) locations of ρ_{max} and ρ_{co}, and b) associated maximum and minimum energies as function of the central density in LHD at constant toroidal ray deflection of – 0.8 m and various values of ω/ω_c (0).

neglecting ray refraction. We have used a polynomial fit to these dependencies to calculate the local values of ω/ω_c, $(\omega/\omega_c)_{co}$, and $(\omega/\omega_c)_{max}$. For the density profile we take $n_e(\rho) = n_e(0)\cdot[1-(\rho)^4]$. In Fig. 17 we show the results for $\omega_p^2/\omega_c^2(0)=0.125$ and $\omega/\omega_c(0)=1.3$ The situation here is similar to a tokamak as the magnetic field is continuously increasing along the ray. Only $N_{||}$ shows a different behavior going through a minimum. In the example of Fig. 17 we also first find an intersection with the $(\omega/\omega_c)_{max}$ - line and later the intersection with the $(\omega/\omega_c)_{co}$ - line, i.e. an absorption window exists. A summary for different magnetic fields and densities, but constant launch angle, is shown in Fig. 18. Here too we find that with increasing magnetic field the absorption zone shifts from high field side off-axis to the center. Taking $(V_{||}^2)_{min}$ = 0.05 as a limit for the availability of a sufficient number of resonant electrons, as we did in comparing Fig. 9b with Fig.5 where the local temperature was 1.5 keV, we find for the accessible range of central electron densities $n_e(0) \leq 7\cdot10^{18}$ m^{-3}. This density range will expand with a higher local temperature and an increasing number of electrons at higher parallel velocities. However, according to Eq. (9) there remains a limit,

independent of temperature, of $\omega_p^2/\omega_c^2 = 0.2$ for an assumed $N_{||}(\rho) \approx 0.6$, corresponding to $n_e(\rho) \leq 1 \cdot 10^{13}$ m^{-3} for $\omega/\omega_c(0)=1.3$ and the given frequency of 84 GHz.

7. Summary

For the extraordinary mode launched from the low field side an absorption is already possible at the cutoff, without the necessity to reach the cyclotron layer, due to the Doppler shifted electron wave interaction. However, there is a severe limit for ω_p^2/ω_c^2 beyond which no absorption is possible. Therefore, in present day tokamaks with a moderate magnetic field the application is restricted to fairly low densities. But as this density limit scales with ω_c^2, it leads to reasonable densities in high magnetic field devices. In such devides the scheme can be applied for off-axis current drive.

Acknowledgement:

This study was partly done during an invited visit of one of the authors to the ECRH group of the National Institute for Fusion Science, Toki, Japan, which is respectfully acknowledged.

The UKAEA Government Division Fusion gave kindly permission to use their BANDIT-3D code.

References:

[1] Erckmann V., Gasparino U., Plasma Phys. Contr. Fusion **39** (1994) 1869.

[2] Harvey R.W. et al., Nuclear Fusion **37** (1997) 69.

[3] Beckmann M., Leuterer F., 11th Workshop on ECE and ECRH, Oh-arai, Japan, 1999, to be published in Fusion Engineering and Design.

[4] Maehara T. et al., Nuclear Fusion **38** (1998) 39.

[5] Maekawa T. et al., Phys. Rev. Lett. **70** (1993) 2561.

[6] O'Brien M.R. et al., in Simulation and Modeling of Thermo-nuclear Plasma, Proc. Tech. Comm. Mtg., Montreal 1992, IAEA, Vienna (1993).

Recent Issues of NIFS Series

NIFS-561 A Fujisawa, H Iguchi, S Lee, K. Tanaka, T Minami, Y Yoshimura, M Osakabe, K Matsuoka, S Okamura, H Idei S Kubo S Ohdachi, S Morita, R Akiyama, K Toi, H Sanuki, K Itoh, K Ida, A Shimizu, S Takagi, C Takahashi, M Kojima, S Hidekuma S Nishimura, M Isobe, A Ejiri, N Inoue, R Sakamoto, Y Hamada and M Fujiwara.
Dynamic Behavior Associated with Electric Field Transitions in CHS Heliotron/Torsatron, Oct 1998
(IAEA-CN-69/EX5/1)

NIFS-562 S Yoshikawa,
Next Generation Toroidal Devices; Oct 1998

NIFS-563 Y Todo and T. Sato,
Kinetic-Magnetohydrodynamic Simulation Study of Fast Ions and Toroidal Alfvén Eigenmodes; Oct 1998
(IAEA-CN-69/THP2/22)

NIFS-564 T. Watari, T. Shimozuma, Y Takeiri, R Kumazawa, T Mutoh, M Sato, O Kaneko, K Ohkubo, S Kubo, H. Idei, Y Oka M Osakabe, T Seki, K Tsumori, Y. Yoshimura, R Akiyama, T Kawamoto, S Kobayashi, F Shimpo, Y Takita, E Asano, S Itoh, G Nomura, T. Ido, M. Hamabe, M Fujiwara, A Iiyoshi, S Morimoto, T Bigelow and Y P. Zhao,
Steady State Heating Technology Development for LHD, Oct. 1998
(IAEA-CN-69/FTP/21)

NIFS-565 A. Sagara, K Y. Watanabe, K Yamazaki, O Motojima, M Fujiwara, O. Mitarai, S. Imagawa, H Yamanishi, H Chikaraishi, A Kohyama, H. Matsui, T. Muroga, T. Noda, N. Ohyabu, T Satow, A A. Shishkin, S. Tanaka, T Terai and T Uda,
LHD-Type Compact Helical Reactors; Oct 1998
(IAEA-CN-69/FTP/03(R)

NIFS-566 N. Nakajima, J Chen, K Ichiguchi and M. Okamoto,
Global Mode Analysis of Ideal MHD Modes in L=2 Heliotron/Torsatron Systems, Oct 1998
(IAEA-CN-69/THP1/08)

NIFS-567 K Ida, M. Osakabe, K Tanaka, T. Minami, S. Nishimura, S. Okamura, A. Fujisawa, Y Yoshimura, S Kubo, R Akiyama, D S.Darrow, H Idei, H. Iguchi, M. Isobe, S Kado, T. Kondo, S Lee, K. Matsuoka, S Morita, I Nomura, S. Ohdachi, M. Sasao, A Shimizu, K. Tumon, S. Takayama, M Takechi, S Takagi, C Takahashi, K. Toi and T. Watari,
Transition from L Mode to High Ion Temperature Mode in CHS Heliotron/Torsatron Plasmas, Oct 1998
(IAEA-CN-69/EX2/2)

NIFS-568 S Okamura, K Matsuoka, R Akiyama, D.S Darrow, A Ejiri, A. Fujisawa, M. Fujiwara, M. Goto, K Ida H Idei, H Iguchi, N Inoue, M Isobe, K. Itoh, S Kado, K. Khlopenkov, T. Kondo, S Kubo, A Lazaros, S Lee, G Matsunaga, T Minami, S Morita, S Murakami, N. Nakajima, N. Nikai, S. Nishimura, I. Nomura, S. Ohdachi, K Ohkuni, M Osakabe, R Pavlichenko, B Peterson, R Sakamoto, H: Sanuki, M. Sasao, A Shimizu, Y. Shirai, S. Sudo, S. Takagi, C Takahashi, S. Takayama, M Takechi, K Tanaka, K Toi, K. Yamazaki, Y. Yoshimura and T Watari,
Confinement Physics Study in a Small Low-Aspect-Ratio Helical Device CHS, Oct 1998
(IAEA-CN-69/OV4/5)

NIFS-569 M.M. Skoric, T Sato, A. Maluckov, M S. Jovanovic,
Micro- and Macro-scale Self-organization in a Dissipative Plasma, Oct 1998

NIFS-570 T Hayashi, N Mizuguchi, T-H. Watanabe, T Sato and the Complexity Simulation Group,
Nonlinear Simulations of Internal Reconnection Event in Spherical Tokamak, Oct 1998
(IAEA-CN-69/TH3/3)

NIFS-571 A Iiyoshi, A Komori, A. Ejiri, M. Emoto, H. Funaba, M Goto, K. Ida, H Idei, S Inagaki, S Kado, O. Kaneko, K. Kawahata, S Kubo R Kumazawa, S. Masuzaki, T. Minami, J. Miyazawa, T Morisaki, S Morita, S Murakami, S Muto, T Muto, Y Nagayama Y Nakamura, H. Nakanishi, K Narihara, K. Nishimura, N Noda, T Kobuchi, S Ohdachi, N Ohyabu, Y Oka, M Osakabe T Ozaki, B.J Peterson, A Sagara, S Sakakibara, R Sakamoto, H Sasao, M Sasao, K Sato, M Sato, T Seki, T Shimozuma M Shoji, H Suzuki, Y Takeiri, K. Tanaka, K. Toi, T. Tokuzawa, K. Tsumori, I. Yamada, H Yamada, S Yamaguchi, M Yokoyama, K Y Watanabe, T. Watari, R. Akiyama, H Chikaraishi, K. Haba, S. Hamaguchi, S. Iima, S Imagawa, N. Inoue K Iwamoto, S Kitagawa, Y. Kubota, J. Kodaira, R. Maekawa, T. Mito T Nagasaka, A. Nishimura Y. Takita, C Takahashi, K Takahata, K Yamauchi, H Tamura, T. Tsuzuki, S Yamada, N Yanagi, H Yonezu, Y Hamada, K Matsuoka, K. Murai K Ohkubo, I Ohtake M. Okamoto, S. Sato, T Satow, S Sudo, S. Tanahashi, K Yamazaki, M Fujiwara and O Motojima,
An Overview of the Large Helical Device Project; Oct 1998
(IAEA-CN-69/OV1/4)

NIFS-572 M Fujiwara, H. Yamada, A Ejiri, M. Emoto, H. Funaba, M Goto, K Ida, H Idei, S. Inagaki, S Kado, O Kaneko, K Kawahata, A Komori, S Kubo, R. Kumazawa, S. Masuzaki, T Minami, J. Miyazawa, T. Morisaki, S Morita, S Murakami, S Muto, T. Muto, Y Nagayama, Y. Nakamura, H. Nakanishi, K. Narihara, K Nishimura, N Noda, T Kobuchi, S Ohdachi, N Ohyabu Y Oka, M Osakabe, T. Ozaki, B J Peterson, A Sagara, S. Sakakibara, R Sakamoto, H Sasao, M. Sasao, K Sato, M Sato, T Seki, T Shimozuma, M Shoji, H Sazuki, Y. Takeiri, K. Tanaka, K Toi, T Tokuzawa, K Tsumori, I Yamada, S Yamaguchi, M Yokoyama, K.Y Watanabe, T Watari, R. Akiyama, H. Chikaraishi, K Haba, S Hamaguchi, M Iima, S Imagawa, N Inoue K Iwamoto, S. Kitagawa, Y. Kubota, J. Kodaira, R. Maekawa, T. Mito, T. Nagasaka, A Nishimura, Y Takita, C Takahashi, K Takahata, K. Yamauchi, H Tamura, T Tsuzuki, S Yamada, N Yanagi, H. Yonezu, Y Hamada, K. Matsuoka, K Murai, K Ohkubo, I Ohtake, M. Okamoto, S Sato, T Satow, S Sudo, S Tanahashi, K Yamazaki, O. Motojima and A Iiyoshi,
Plasma Confinement Studies in LHD; Oct. 1998

(IAEA-CN-69/EX2/3)

NIFS-573 O. Motojima, K. Akaishi, H. Chikaraishi, H. Funaba, S Hamaguchi, S. Imagawa, S. Inagaki, N. Inoue, A. Iwamoto, S Kitagawa, A. Komori, Y. Kubota, R. Maekawa, S. Masuzaki, T. Mito, J. Miyazawa, T. Morisaki, T. Muroga, T. Nagasaka, Y. Nakamura, A. Nishimura, K. Nishimura, N. Noda, N. Ohyabu, S. Sagara, S. Sakakibara, R Sakamoto, S. Satoh, T. Satow, M Shoji, H Suzuki, K. Takahata, H. Tamura, K. Watanabe, H. Yamada, S. Yamada, S Yamaguchi, K. Yamazaki, N. Yanagi, T. Baba, H. Hayashi, M. Iima, T. Inoue, S. Kato, T. Kato, T. Kondo, S. Moriuchi, H. Ogawa, I. Ohtake, K. Ooba, H. Sekiguchi, N. Suzuki, S. Takami, Y. Taniguchi, T. Tsuzuki, N. Yamamoto, K. Yasui, H. Yonezu, M. Fujiwara and A. Iiyoshi,
Progress Summary of LHD Engineering Design and Construction; Oct. 1998
(IAEA-CN-69/FT2/1)

NIFS-574 K. Toi, M. Takechi, S. Takagi, G. Matsunaga, M. Isobe, T. Kondo, M. Sasao, D.S. Darrow, K. Ohkuni, S. Ohdachi, R. Akiyama A. Fujisawa, M. Gotoh, H. Idei, K. Ida, H. Iguchi, S. Kado, M. Kojima, S. Kubo, S. Lee, K. Matsuoka, T. Minami, S Morita, N. Nikai, S Nishimura, S. Okamura, M. Osakabe, A. Shimizu, Y. Shirai, C. Takahashi, K. Tanaka, T. Watari and Y. Yoshimura.
Global MHD Modes Excited by Energetic Ions in Heliotron/Torsatron Plasmas;Oct. 1998
(IAEA-CN-69/EXP1/19)

NIFS-575 Y. Hamada, A. Nishizawa, Y. Kawasumi, A. Fujisawa, M Kojima, K. Narihara, K. Ida, A. Ejiri, S Ohdachi, K. Kawahata, K. Toi, K. Sato, T. Seki, H. Iguchi, K. Adachi, S. Hidekuma, S.Hirokura, K. Iwasaki, T. Ido, R. Kumazawa, H. Kuramoto, T Minami, I.. Nomura, M. Sasao, K.N. Sato, T. Tsuzuki, I. Yamada and T. Watari,
Potential Turbulence in Tokamak Plasmas;Oct. 1998
(IAEA-CN-69/EXP2/14)

NIFS-576 S. Murakami, U. Gasparino, H. Idei, S. Kubo, H. Maassberg, N. Marushchenko, N. Nakajima, M. Romé and M. Okamoto.
5D Simulation Study of Suprathermal Electron Transport in Non-Axisymmetric Plasmas;Oct. 1998
(IAEA-CN-69/THP1/01)

NIFS-577 S. Fujiwara and T. Sato,
Molecular Dynamics Simulation of Structure Formation of Short Chain Molecules, Nov 1998

NIFS-578 T. Yamagishi,
Eigenfunctions for Vlasov Equation in Multi-species Plasmas Nov. 1998

NIFS-579 M. Tanaka, A. Yu Grosberg and T. Tanaka,
Molecular Dynamics of Strongly-Coupled Multichain Coulomb Polymers in Pure and Salt Aqueous Solutions;Nov. 1998

NIFS-580 J. Chen, N. Nakajima and M. Okamoto,
Global Mode Analysis of Ideal MHD Modes in a Heliotron/Torsatron System: I. Mercier-unstable Equilibria,Dec. 1998

NIFS-581 M. Tanaka, A. Yu Grosberg and T. Tanaka,
Comparison of Multichain Coulomb Polymers in Isolated and Periodic Systems: Molecular Dynamics Study; Jan. 1999

NIFS-582 V.S Chan and S. Murakami,
Self-Consistent Electric Field Effect on Electron Transport of ECH Plasmas; Feb. 1999

NIFS-583 M. Yokoyama, N. Nakajima, M. Okamoto, Y. Nakamura and M. Wakatani,
Roles of Bumpy Field on Collisionless Particle Confinement in Helical-Axis Heliotrons;Feb 1999

NIFS-584 T.-H. Watanabe, T. Hayashi, T. Sato, M. Yamada and H Ji,
Modeling of Magnetic Island Formation in Magnetic Reconnection Experiment,Feb 1999

NIFS-585 R. Kumazawa, T. Mutoh, T. Seki, F. Shinpo, G. Nomura, T. Ido, T Watari, Jean-Marie Noterdaeme and Yangping Zhao,
Liquid Stub Tuner for Ion Cyclotron Heating;Mar. 1999

NIFS-586 A Sagara, M Iima, S. Inagaki, N. Inoue, H. Suzuki, K. Tsuzuki, S. Masuzaki, J. Miyazawa, S. Morita, Y Nakamura, N. Noda, B Peterson, S. Sakakibara, T. Shimozuma, H. Yamada, K. Akaishi, H. Chikaraishi, H. Funaba, O. Kaneko, K Kawahata, A. Komori, N. Ohyabu, O. Motojima, LHD Exp. Group 1, LHD Exp. Group 2,
Wall Conditioning at the Starting Phase of LHD;Mar. 1999

NIFS-587 T. Nakamura and T. Yabe,
Cubic Interpolated Propagation Scheme for Solving the Hyper-Dimensional Vlasov-Poisson Equation in Phase Space;Mar. 1999

NIFS-588 W.X. Wnag, N. Nakajima, S. Murakami and M. Okamoto,
An Accurate

δf Method for Neoclassical Transport Calculation, Mar 1999

NIFS-589 K Kishida, K Araki, S Kishiba and K Suzuki,
Local or Nonlocal? Orthonormal Divergence-free Wavelet Analysis of Nonlinear Interactions in Turbulence, Mar 1999

NIFS-590 K Araki, K Suzuki, K Kishida and S Kishiba,
Multiresolution Approximation of the Vector Fields on T^3, Mar. 1999

NIFS-591 K. Yamazaki, H Yamada, K Y Watanabe, K Nishimura, S Yamaguchi, H Nakanishi, A Komori, H Suzuki, T Mito, H. Chikaraishi, K Murai, O Motojima and the LHD Group,
Overview of the Large Helical Device (LHD) Control System and Its First Operation, Apr 1999

NIFS-592 T Takahashi and Y Nakao,
Thermonuclear Reactivity of D-T Fusion Plasma with Spin-Polarized Fuel, Apr 1999

NIFS-593 H. Sugama,
Damping of Toroidal Ion Temperature Gradient Modes, Apr 1999

NIFS-594 Xiaodong Li,
Analysis of Crowbar Action of High Voltage DC Power Supply in the LHD ICRF System, Apr 1999

NIFS-595 K Nishimura, R. Horiuchi and T. Sato,
Drift-kink Instability Induced by Beam Ions in Field-reversed Configurations, Apr 1999

NIFS-596 Y Suzuki, T-H. Watanabe, T. Sato and T Hayashi,
Three-dimensional Simulation Study of Compact Toroid Plasmoid Injection into Magnetized Plasmas; Apr. 1999

NIFS-597 H. Sanuki, K. Itoh, M Yokoyama, A Fujisawa, K. Ida, S. Toda, S -I. Itoh, M Yagi and A Fukuyama,
Possibility of Internal Transport Barrier Formation and Electric Field Bifurcation in LHD Plasma, May 1999

NIFS-598 S. Nakazawa, N. Nakajima, M. Okamoto and N. Ohyabu,
One Dimensional Simulation on Stability of Detached Plasma in a Tokamak Divertor, June 1999

NIFS-599 S Murakami, N Nakajima, M Okamoto and J. Nhrenberg,
Effect of Energetic Ion Loss on ICRF Heating Efficiency and Energy Confinement Time in Heliotrons June 1999

NIFS-600 R Horiuchi and T. Sato,
Three-Dimensional Particle Simulation of Plasma Instabilities and Collisionless Reconnection in a Current Sheet;; June 1999

NIFS-601 W. Wang, M Okamoto, N. Nakajima and S Murakami,
Collisional Transport in a Plasma with Steep Gradients; June 1999

NIFS-602 T. Mutoh, R Kumazawa, T Saki, K. Saito, F. Simpo, G. Nomura, T Watari, X. Jikang, G Cattanei, H Okada, K Ohkubo, M Sato, S. Kubo, T. Shimozuma, H. Idei, Y. Yoshimura, O. Kaneko, Y. Takeiri, M. Osakabe, Y. Oka, K Tsumori, A Komori, H Yamada, K Watanabe, S. Sakakibara, M Shoji, R. Sakamoto, S Inagaki, J Miyazawa, S Morita, K Tanaka, B.J Peterson, S Murakami, T Minami, S Ohdachi, S. Kado, K. Nanhara, H. Sasao, H Suzuki, K. Kawahata, N Ohyabu, Y Nakamura, H. Funaba, S Masuzaki, S Muto, K. Sato, T. Morisaki, S. Sudo, Y Nagayama, T. Watanabe, M Sasao, K Ida, N Noda, K. Yamazaki, K Akaishi, A Sagara, K Nishimura, T Ozaki, K. Toi, O. Motojima, M Fujiwara, A Iiyoshi and LHD Exp Group 1 and 2,
First ICRF Heating Experiment in the Large Helical Device; July 1999

NIFS-603 P C de Vries, Y. Nagayama, K. Kawahata, S Inagaki, H Sasao and K Nagasaki,
Polarization of Electron Cyclotron Emission Spectra in LHD, July 1999

NIFS-604 W. Wang, N Nakajima, M. Okamoto and S. Murakami,
δf Simulation of Ion Neoclassical Transport; July 1999

NIFS-605 T. Hayashi, N. Mizuguchi, T Sato and the Complexity Simulation Group,
Numerical Simulation of Internal Reconnection Event in Spherical Tokamak, July 1999

NIFS-606 M Okamoto, N Nakajima and W Wang,
On the Two Weighting Scheme

for δf Collisional Transport Simulation, Aug. 1999

NIFS-607 O. Motojima, A.A. Shishkin, S. Inagaki, K. Y. Watanabe,
Possible Control Scenario of Radial Electric Field by Loss-Cone-Particle Injection into Helical Device, Aug. 1999

NIFS-608 R. Tanaka, T. Nakamura and T. Yabe,
Constructing Exactly Conservative Scheme in Non-conservative Form; Aug. 1999

NIFS-609 H. Sugama,
Gyrokinetic Field Theory; Aug. 1999

NIFS-610 M. Takechi, G. Matsunaga, S. Takagi, K.Ohkuni, K. Toi, M. Osakabe, M. Isobe, S. Okamura, K. Matsuoka, A Fujisawa, H Iguchi, S. Lee, T. Minami, K. Tanaka, Y Yoshimura and CHS Group,
Core Localized Toroidal Alfven Eigenmodes Destabilized By Energetic Ions in the CHS Heliotron/Torsatron, Sep 1999

NIFS-611 K. Ichiguchi,
MHD Equilibrium and Stability in Heliotron Plasmas; Sep. 1999

NIFS-612 Y. Sato, M. Yokoyama, M. Wakatani and V. D. Pusovitov,
Complete Suppression of Pfirsch-Schluter Current in a Toroidal l=3 Stellarator; Oct. 1999

NIFS-613 S. Wang, H. Sanuki and H. Sugama,
Reduced Drift Kinetic Equation for Neoclassical Transport of Helical Plasmas in Ultra-low Collisionality Regime; Oct. 1999

NIFS-614 J. Miyazawa, H. Yamada, K. Yasui, S Kato, N . Fukumoto, M. Nagata and T Uyama,
Design of Spheromak Injector Using Conical Accelerator for Large Helical Device, Nov. 1999

NIFS-615 M. Uchida, A. Fukuyama, K Itoh, S.-I Itoh and M. Yagi,
Analysis of Current Diffusive Ballooning Mode in Tokamaks; Dec. 1999

NIFS-616 M. Tanaka, A.Yu Grosberg and T. Tanaka,
Condensation and Swelling Behavior of Randomly Charged Multichain Polymers by Molecular Dynamics Simulations; Dec. 1999

NIFS-617 S. Goto and S. Kida,
Sparseness of Nonlinear Coupling; Dec 1999

NIFS-618 M.M. Skoric, T Sato, A. Maluckov and M.S. Jovanovic,
;
Complexity in Laser Plasma Instabilities Dec. 1999

NIFS-619 T.-H Watanabe, H. Sugama and T. Sato,
Non-dissipative Kinetic Simulation and Analytical Solution of Three-mode Equations of Ion Temperature Gradient Instability; Dec. 1999

NIFS-620 Y. Oka, Y. Takeiri, Yu.I.Belchenko, M. Hamabe, O. Kaneko, K Tsumori, M Osakabe, E Asano, T Kawamoto, R. Akiyama,
Optimization of Cs Deposition in the 1/3 Scale Hydrogen Negative Ion Source for LHD-NBI System Dec 1999

NIFS-621 Yu.I. Belchenko, Y. Oka, O Kaneko, Y. Takein, A Krivenko, M. Osakabe, K. Tsumori, E Asano, T Kawamoto, R. Akiyama,
Recovery of Cesium in the Hydrogen Negative Ion Sources; Dec 1999

NIFS-622 Y. Oka, O. Kaneko, K. Tsumori, Y. Takeiri, M. Osakabe, T. Kawamoto, E. Asano, and R. Akiyama
H- Ion Source Using a Localized Virtual Magnetic Filter in the Plasma Electrode: Type I LV Magnetic Filter: Dec. 1999

NIFS-623 M. Tanaka, S Kida, S. Yanase and G. Kawahara,
Zero-absolute-vorticity State in a Rotating Turbulent Shear Flow; Jan 2000

NIFS-624 F. Leuterer, S. Kubo,
Electron Cyclotron Current Drive at $\omega \approx \omega_c$ with X-mode Launched from the Low Field Side; Feb. 2000